Supporting Information

S.1 Full Experimental Results

Table S 1: Sample weights and calculated yields for experimental work.

Sample No.	Dried Weight (g)	Calcined Mass (g)	Organics Mass (g)	Organics Content (%)	Yield (%)
1-1	0.49	0.019	0.474	96	13
1-2	9.01	0.526	8.479	94	78
1-3	0.00	0.000	0.004	100	0
1-4	1.07	0.565	0.503	47	84
1-5	0.80	0.015	0.788	98	9
1-6	10.54	0.438	10.099	96	57
1-7	0.02	0.008	0.012	61	5
1-8	1.26	0.712	0.547	43	94
1-9	1.40	0.047	1.352	97	29
1-10	10.91	0.489	10.420	96	82
1-11	0.15	0.065	0.090	58	40
1-12	1.26	0.543	0.712	57	81
1-13	1.47	0.048	1.422	97	30
1-14	13.23	0.573	12.655	96	80
1-15	0.14	0.063	0.078	56	39
1-16	0.96	0.440	0.521	54	58
2-1	1.20	0.52	0.68	56	87
2-2	0.57	0.28	0.29	50	47
2-3	0.26	0.10	0.16	63	16
2-4	1.30	0.55	0.75	58	91
2-5	0.47	0.23	0.24	50	39
2-6	0.21	0.10	0.11	51	17
3-1	1.14	0.48	0.66	59	80
3-2	1.20	0.47	0.73	61	78
3-3	1.14	0.44	0.69	61	74
3-4	1.19	0.39	0.80	67	65
3-5	1.16	0.49	0.67	58	81
4-1	0.73	0.39	0.34	47	65
4-2	0.84	0.48	0.36	42	80
4-3	0.78	0.42	0.36	46	69
4-4	0.49	0.25	0.25	50	41
4-5	0.87	0.47	0.40	46	78
4-6	0.88	0.51	0.37	42	86
4-7	0.64	0.34	0.30	47	57

Table S 2: Summary of the porosity data for all samples that were characterized by N_2 adsorption and XRD. The variables are fully described in Section 2.3. Comparison is made to available material properties for MCM-41 samples from literature (Samples A, B and C).

Sample No.	**Primary Isotherm Type**	$\mathbf{S_{BET}}$ ($\mathbf{m^2\ g^{-1}}$)	$\mathbf{V_{pore}}$ ($\mathbf{cm^3\ g^{-1}}$)	$\mathbf{d_{pore}}$ **(nm)**	$\mathbf{d_{100}}$ **(nm)**	$\mathbf{a_0}$ **(nm)**	$\mathbf{th_{wall}}$ **(nm)**	$\mathbf{I_{200}/I_{110}}$
A [1, 2]	IV(a)	1040	0.79	4.00	3.98	4.60	0.60	0.62
B [3]	-	-	-	-	3.48	4.02	-	0.65
C [4]	IV(a)	1312	0.86	3.14	3.05	3.52	0.38	0.00
1-2	IV(a)	1120	0.906	2.48	4.03	4.65	2.17	0.00
1-4	IV(a)	1005	0.828	2.45	3.88	4.48	2.03	0.28
1-6	IV(a)	970	0.721	2.51	3.98	4.60	2.09	0.00
1-8	IV(a)	1030	0.839	2.30	3.81	4.40	2.10	0.27
1-10	IV(a)	1181	0.966	2.63	3.80	4.39	1.76	0.00
1-12	IV(b)	1259	0.834	2.12	3.50	4.04	1.92	0.06
1-14	IV(a)	1217	1.003	2.55	3.82	4.41	1.86	0.04
1-16	IV(b)	1210	0.850	2.14	3.68	4.25	2.11	0.08
2-1	IV(b)	1259	0.971	2.31	3.56	4.11	1.80	0.12
2-2	IV(b)	1165	0.841	2.15	3.40	3.93	1.78	0.46
2-3	IV(a)	1159	0.843	2.13	3.44	3.97	1.84	-
2-4	IV(a)	1193	0.857	2.22	3.52	4.06	1.84	0.11
2-5	IV(b)	1144	0.824	2.14	3.43	3.96	1.82	0.50
2-6	IV(a)	1194	0.898	2.25	3.47	4.01	1.76	0.07
3-1	IV(b)	1149	0.789	2.18	3.39	3.91	1.73	0.06
3-2	IV(b)	1203	0.835	2.17	3.38	3.90	1.73	0.00
3-3	IV(b)	1218	0.938	2.40	3.63	4.19	1.79	0.28
3-4	IV(a)	1273	0.969	2.35	-	-	-	0.00
3-5	IV(b)	1218	0.911	2.24	3.50	4.04	1.80	0.20
4-1	IV(b)	983	0.706	2.20	3.55	4.10	1.90	0.52
4-2	IV(b)	961	0.736	2.27	3.68	4.25	1.98	0.49
4-3	IV(b)	926	0.679	2.24	3.67	4.24	1.94	0.00
4-4	IV(b)	1186	0.830	2.09	3.44	3.97	1.88	0.18
4-5	IV(a)	783	0.608	2.80	-	-	-	0.00
4-6	IV(a)	878	0.686	2.74	-	-	-	0.00
4-7	IV(b)	1142	0.841	2.10	3.40	3.93	1.83	0.29

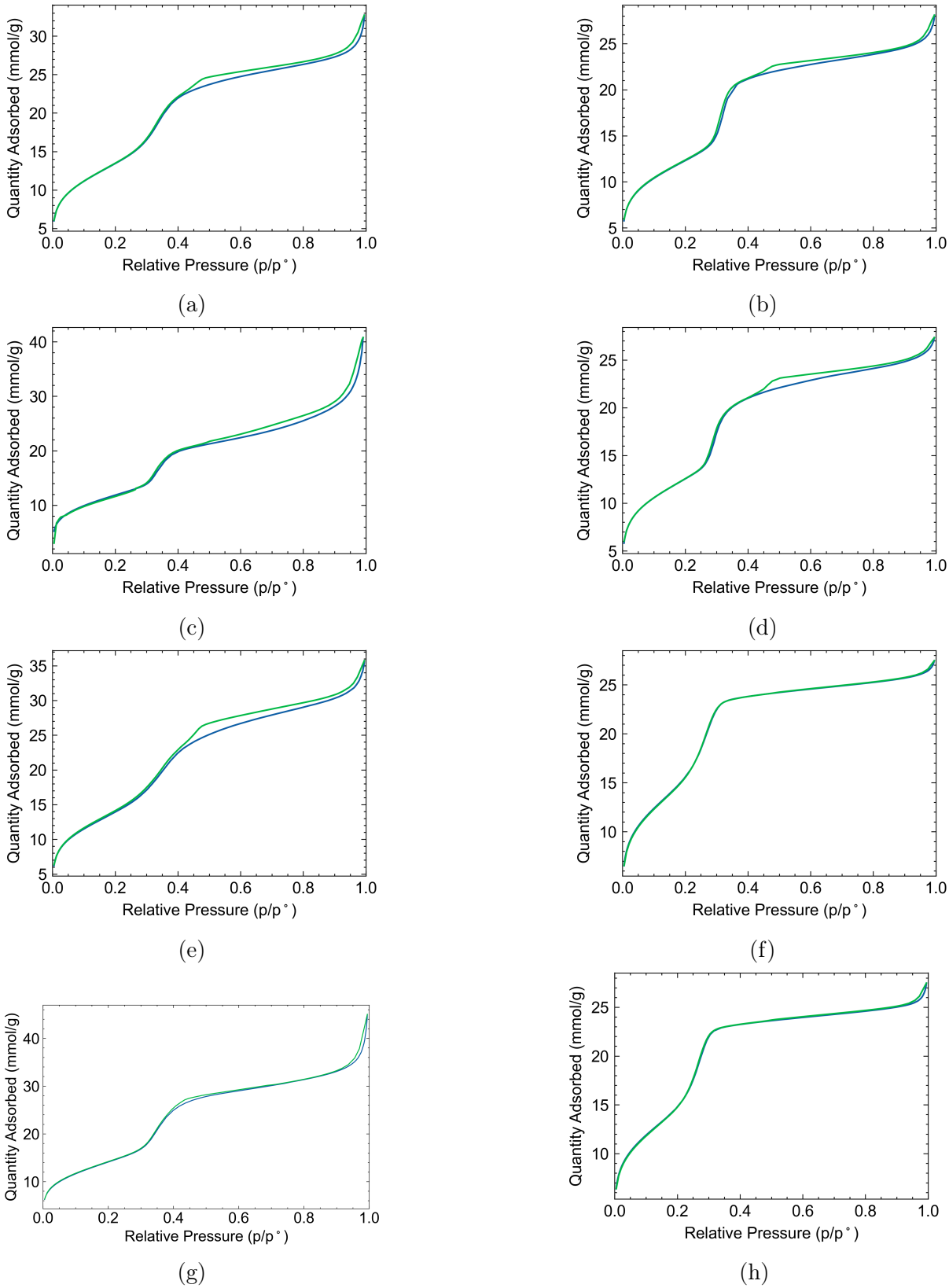

Figure S 1: N_2 adsorption isotherms for two-level four-factor screening samples. Letters a-h represent samples 1-2, 1-4, 1-6, 1-8, 1-10, 1-12, 1-14 and 1-16, sequentially. The blue line indicates adsorption while the green line indicates desorption.

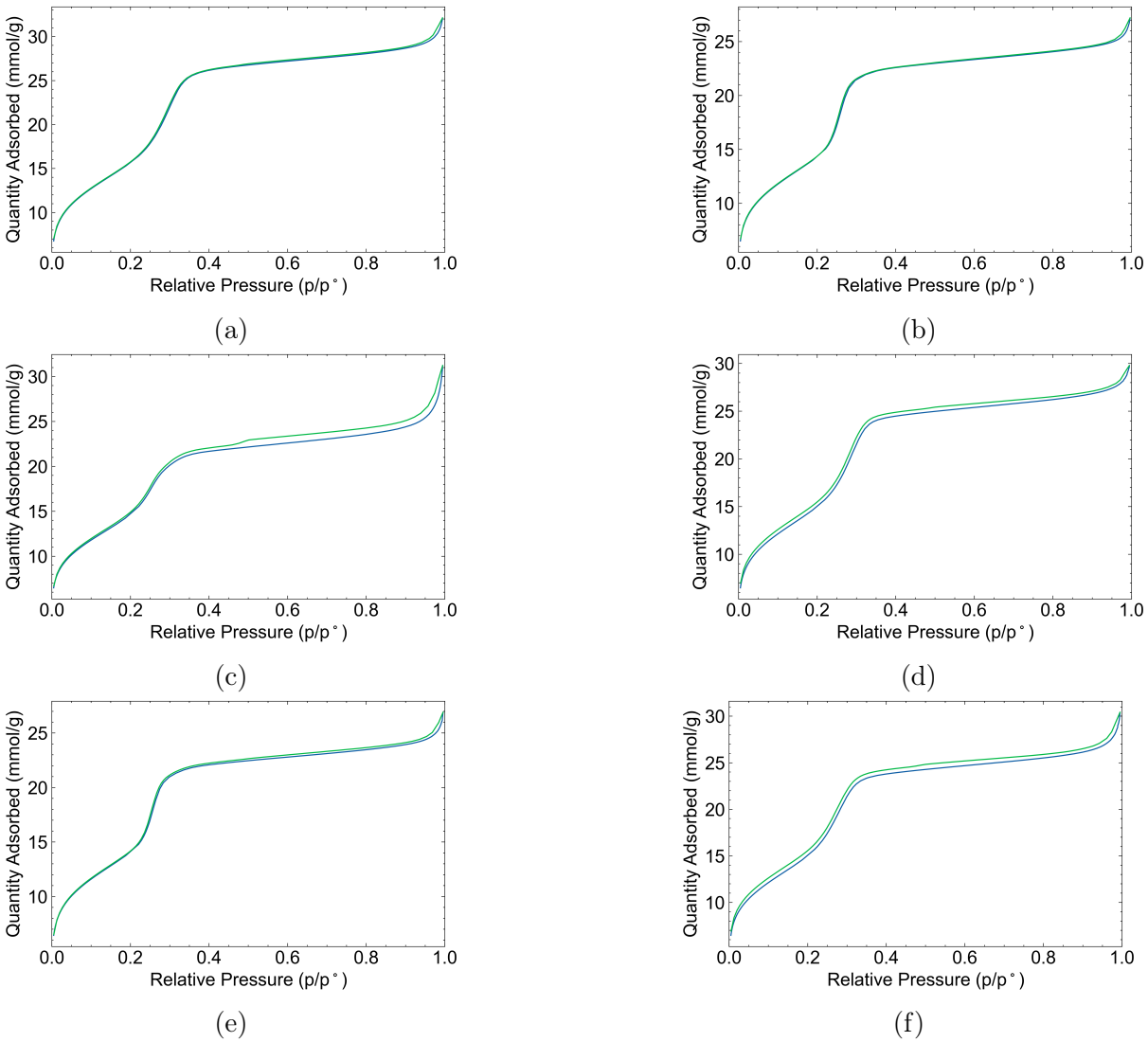

Figure S 2: N_2 adsorption isotherms for component ratio investigation samples. Letters at to f represent samples 2-1 to 2-6, sequentially. The blue line indicates adsorption while the green line indicates desorption.

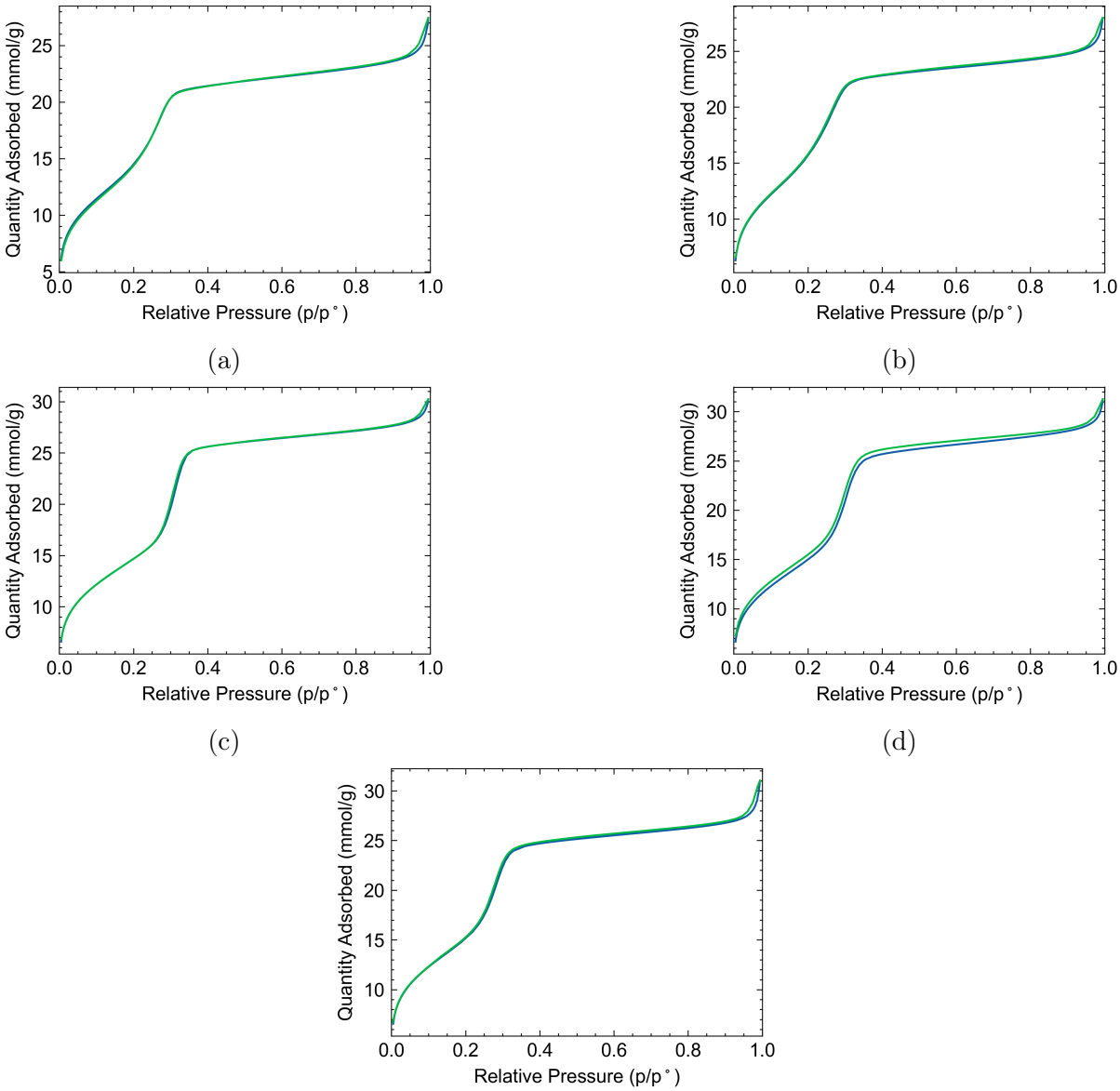

Figure S 3: N_2 adsorption isotherms for additive investigation samples with different additives: (a) L-arginine, (b) ammonia, (c) PEHA, (d) propylamine, (e) no additive.

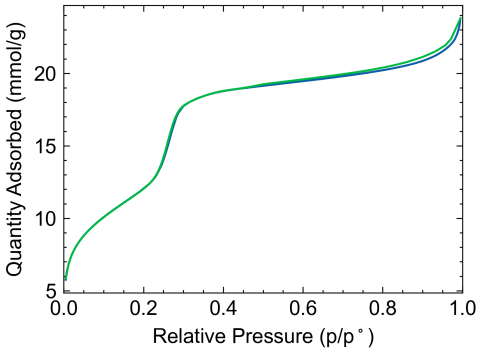

(a)

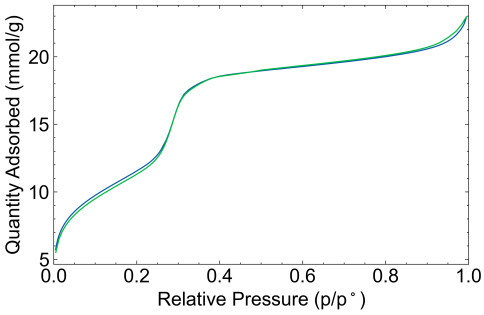

(b)

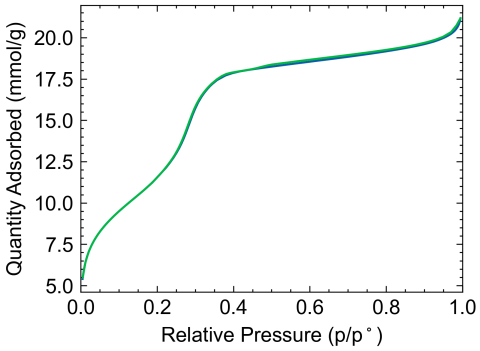

(c)

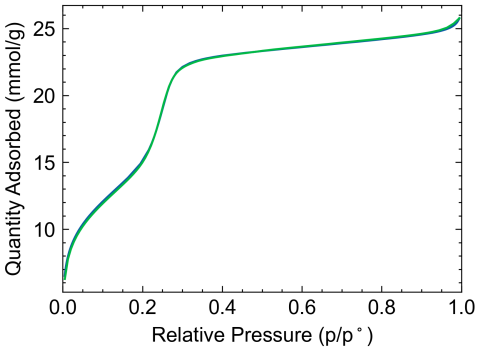

(d)

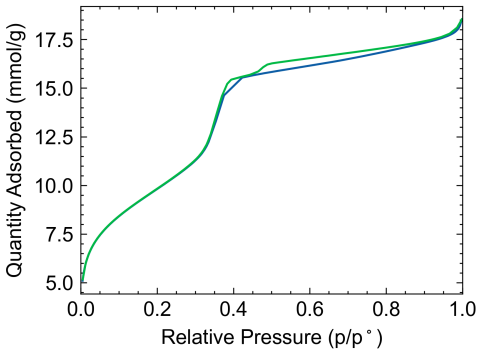

(e)

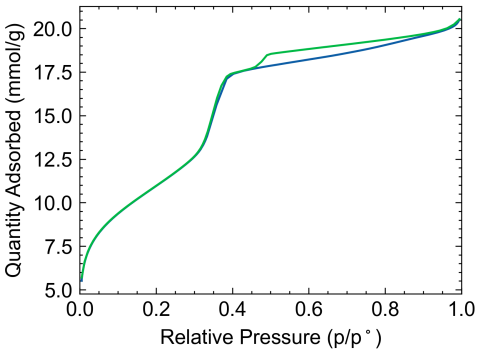

(f)

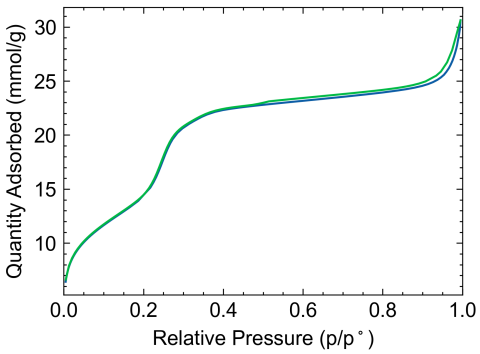

(g)

Figure S 4: N_2 adsorption isotherms for ordered mesoporous silica samples using PEHA as an additive in synthesis. Letters a to g represent samples 4-1 to 4-7, sequentially.

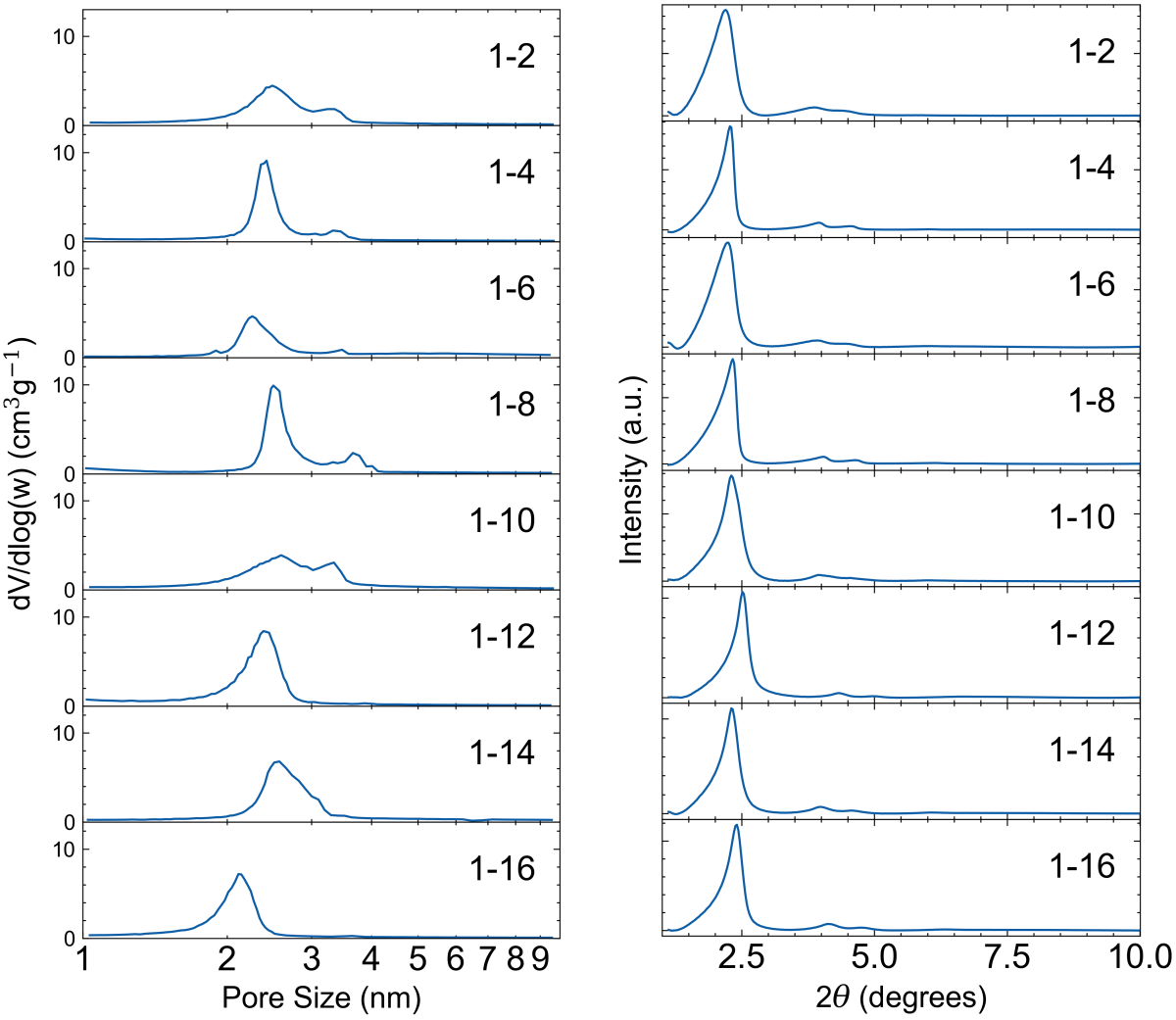

Figure S 5: Pore size distributions (left) and XRD data (right) for two-level four-factor screening samples. For XRD data, baseline intensity was removed manually to allow for easier comparison between peaks.

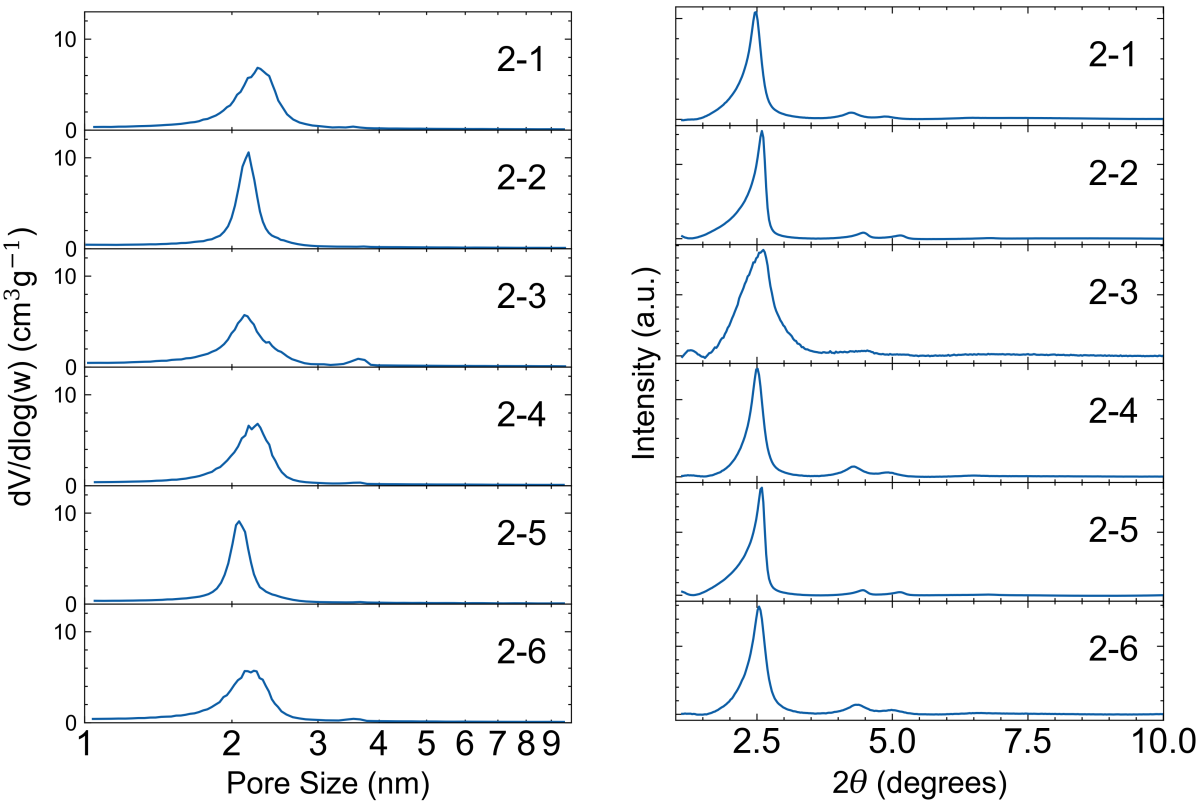

Figure S 6: Pore size distributions (left) and XRD data (right) for component ratio investigation samples. For XRD data, baseline intensity was removed manually to allow for easier comparison between peaks.

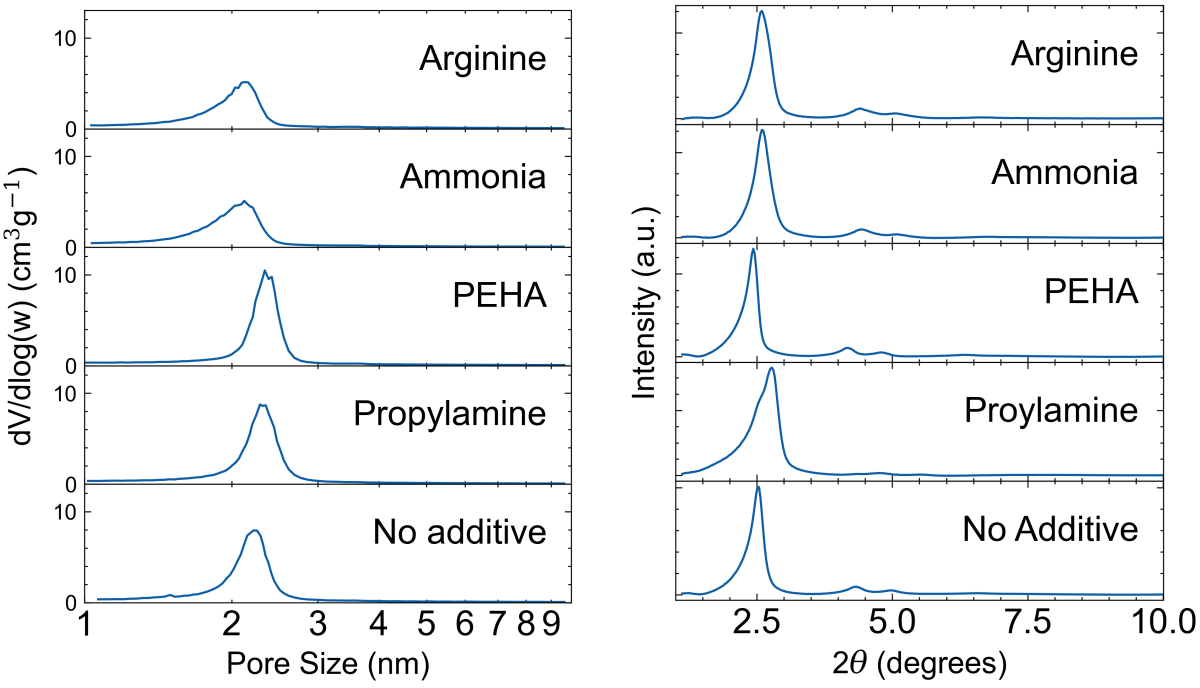

Figure S 7: Pore size distributions (left) and XRD data (right) for investigation with different additives. For XRD data, baseline intensity was removed manually to allow for easier comparison between peaks.

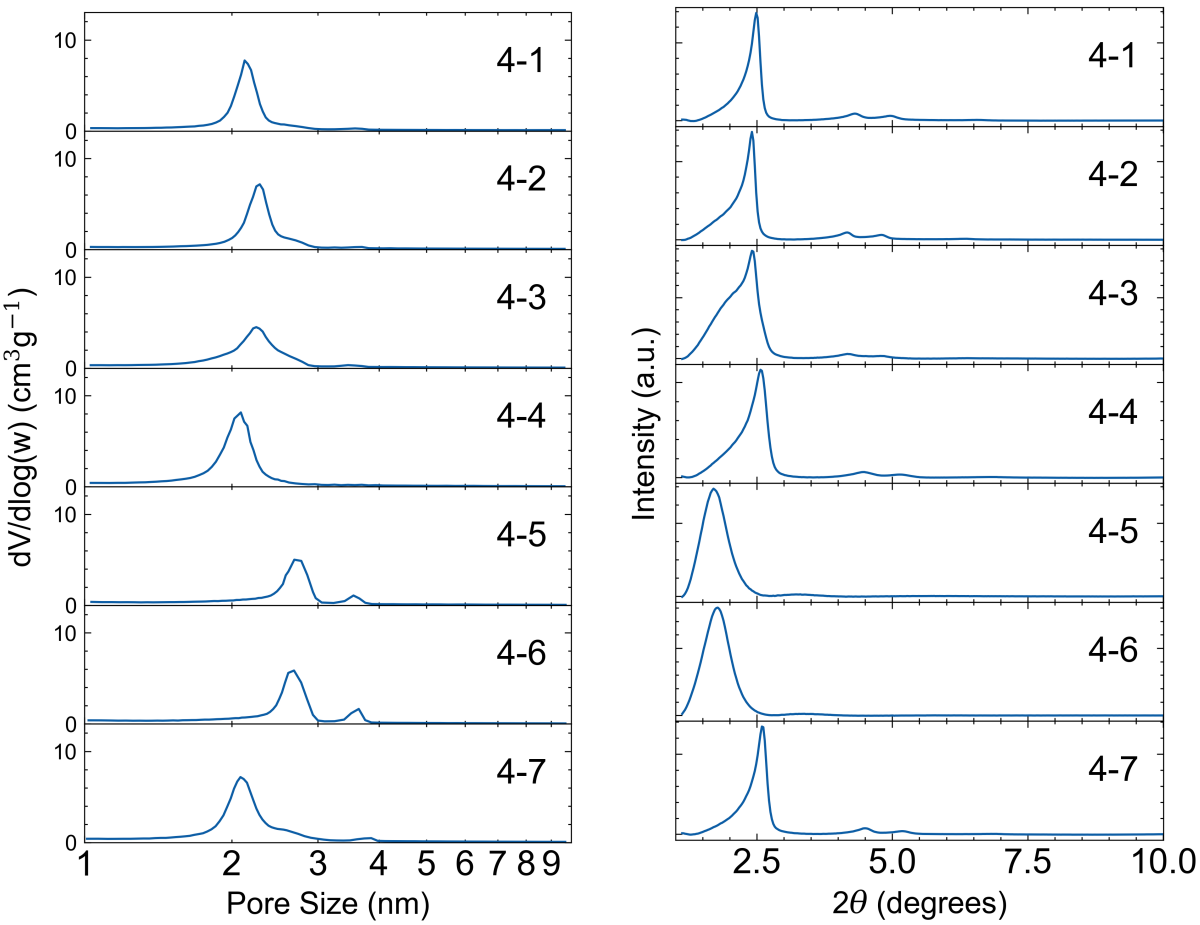

Figure S 8: Pore size distributions (left) and XRD data (right) for samples using PEHA as an additive in synthesis. For XRD data, baseline intensity was removed manually to allow for easier comparison between peaks.

S.2 Uncertainty Analysis

To estimate the uncertainty in results for yield, organic content and material properties of samples in this work, the values obtained for two sets of two samples that were synthesised under the same conditions were compared to give an approximate expected range for results. The first set of samples are 2-1 and 3-1, which were synthesised under the same conditions (see Table 1 of the main paper). The second set of samples (R-1 and R-2) were synthesised under the following conditions: [Si] = 100 mM, Si:N = 2, Si:CTAB = 2, pH = 10.8. For this second set of results, only gas adsorption results were available. The estimated uncertainty for each property is given in the final column of Table S3, which is estimated based on the range of results for both sets of samples (where available). Although a more rigorous analysis, based on multiple repeat experiments would have been desirable, we believe the vaues in Table S3 provide a conservative estimate of the real experimental uncertainty.

Table S 3: Summary of differences in yields, organic contents and material properties obtained for repeat samples synthesised under the same conditions.

Parameter	**R-1**	**R-2**	**Δ**	**2-1**	**3-1**	**Δ**	**Estimated Uncertainty (±)**
Yield (%)	-	-	-	87	80	7	10
Organic Content (%)	-	-	-	56	59	3	5
BET Surface Area (m^2 g^{-1})	1211	1277	66	1159	1149	10	70
Pore Volume (cm^3 g^{-1})	0.958	0.952	0.006	0.843	0.789	0.054	0.06
Pore Diameter (nm)	2.31	2.21	0.1	2.13	2.18	0.05	0.1
Wall Thickness (nm)	-	-	-	1.31	1.21	0.1	0.1
Order Parameter	-	-	-	0.12	0.06	0.06	0.1

S.3 Literature XRD

16

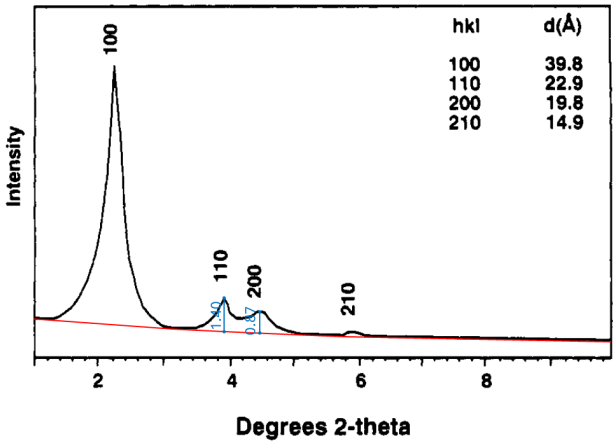

Figure S 9: XRD pattern reported by Beck et al. in the original synthesis of MCM-41, taken from [1]. The red line indicates the baseline reflection from which the relative intensities of peaks (110) and (200) were measured (labelled in blue).

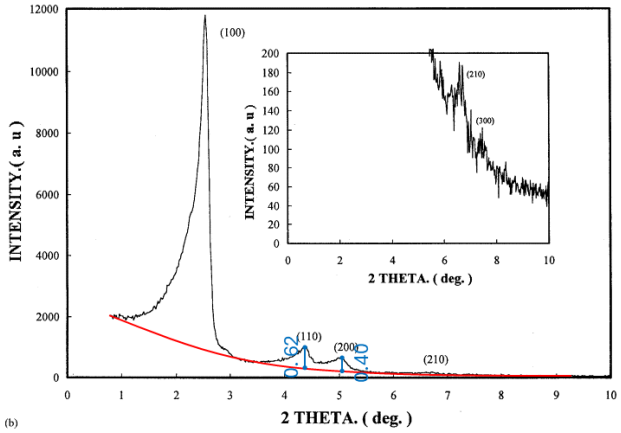

Figure S 10: XRD pattern reported by Cai et al. in their synthesis of MCM-41, taken from [3] for the most well-ordered sample, produced at room temperature. The red line indicates the baseline reflection from which the relative intensities of peaks (110) and (200) were measured (labelled in blue).

S.4 Bio-Inspired Additive Models

Arginine has three ionisation points, corresponding to pKa values of 2.17, 9.04 and 12.48 [5]. The most relevant protonation state in this work is shown as IV in Figure S11, which is present in high proportions (>75%) during HLC self-assembly in the early stages of OMS synthesis. This form has an overall negative charge situated on the carboxylate group of the amino acid backbone. The guanidinium group of the arginine sidechain, which is typically positively charged at physiological pH, becomes deprotonated at high pH.

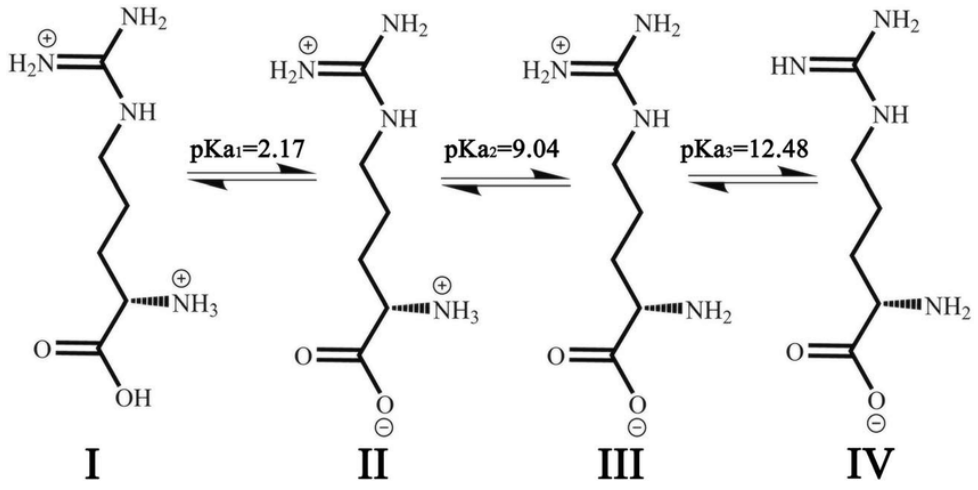

Figure S 11: Diagram of pKa values corresponding to the ionisation of multiple chemical groups in an arginine molecule. Taken from Wang et al. [5].

PEHA's first two ionisation points corresponding to pKa values of 9.7 and 11.0 [6] (shown in Figure S12), refer to protonation of the terminal primary amines. The internal (secondary) amine groups can also protonate, but this happens at pH values that are too low to be relevant in the present context [7]. The most relevant protonation state to this work is when the molecule bears an overall neutral charge with deprotonated amine groups, which occurs at high pH values. The relative composition of different degrees of protonation for both bio-inspired additives between pH 7 and 14 is given in Figure S13.

A mapping for arginine residues in proteins was suggested by the authors of the Martini 3 model [8], which is comprised of 3 beads with the amino acid backbone represented by a single bead (see Figure S14, left). While this is practical for models of proteins that contain many connected backbone beads, for forms of arginine that do not have a zwitterionic backbone, (instead having only either a positively charged amine group or a negatively charged carboxylate group) combining the carboxylate group and the primary amine group into a single bead may not be sufficient to capture the full behaviour of the molecule. Therefore, to more accurately capture this behaviour and allow for the representation of different protonation states of arginine (and in particular the high pH form present during OMS self-assembly), an alternative mapping scheme based on 4 beads is proposed, in which the backbone is divided into two beads, one representing the primary amine group and adjoined carbon, whilst the other represents the charged carboxylate group

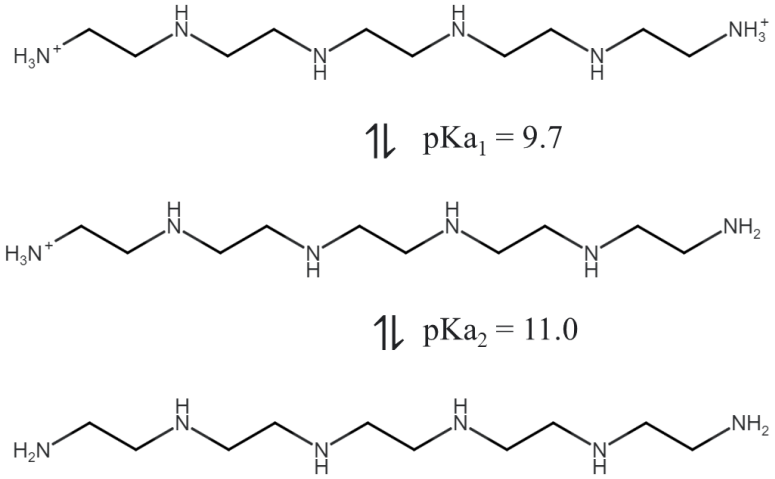

Figure S 12: Diagram of pKa values corresponding to the ionisation of terminal amine groups in PEHA.

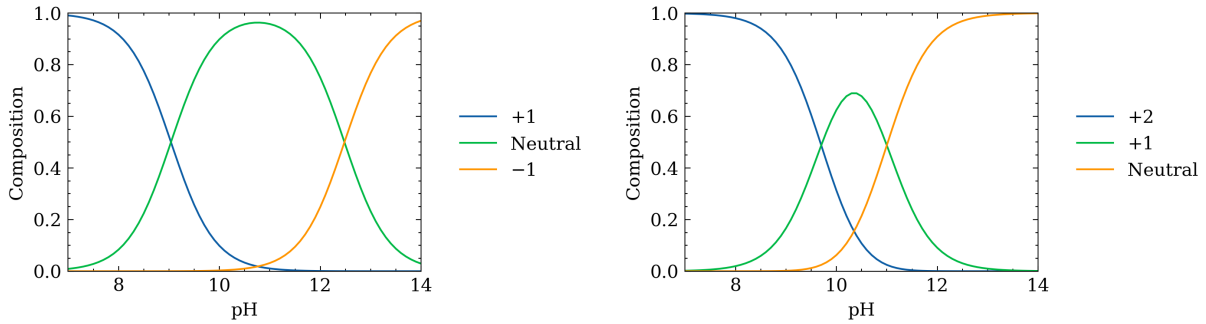

Figure S 13: Distribution of charge states for bio-inspired additives arginine (left) and PEHA (right) between pH 7 and 14. The total molecular charge for each degree of protonation is given in the legend.

(see Figure S14, right). The side chain is mapped with the alkane group represented by one bead with a 3-1 mapping, while the guanidinium group is captured in another bead.

The bead types for the arginine side chain suggested by the Martini 3 authors are the SC3 bead for the alkane chain (ARG_1) and the SQ3p bead for the charged guanidinium group at the end of the side chain (ARG_2). However, to more finely tune the side chain interactions, a recommended approach is to calculate the free energy difference of the side chain beads in different solvents using different candidate bead types, and compare these to experimental values. This procedure was carried out for alternative charged bead types representing the guanidinium group (ARG_2). All small charged bead types were tested using the p label, which represents the hydrogen bonding potential of the group. The two solvents used were water and cyclohexane for which there is experimental data for a neutral analogue of the arginine side chain, *N*-propylguanidine, [9, 10] which gives a free energy of partitioning value of -24.2 kJ mol^{-1}. The free energy of partitioning between water and cyclohexane for the arginine side chain was calculated by thermodynamic integration for each bead. The electrostatic charge of the ARG_2 bead was switched off and only Lennard-

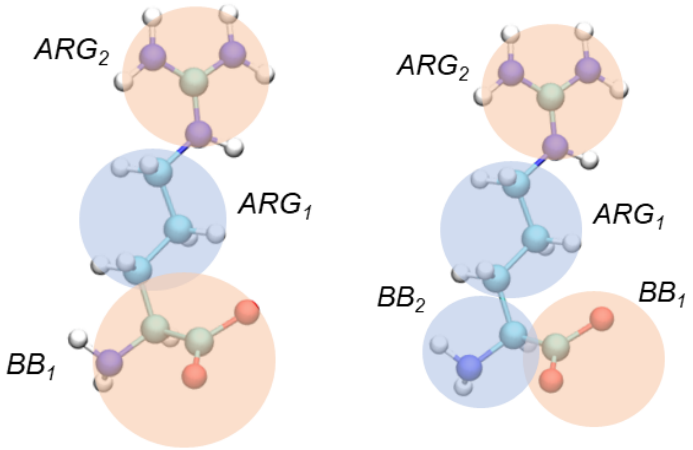

Figure S 14: CG mapping schemes for arginine. The standard Martini 3 mapping scheme is shown on the left while the 4 bead model mapping used in this work is shown on the right.

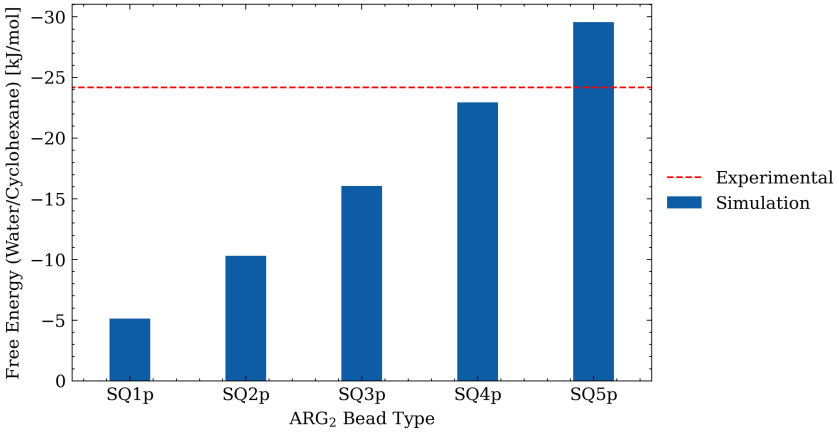

Figure S 15: Partition free energy between water and cyclohexane for different Martini 3 bead types representing the guanidinium group in the arginine side chain analogue.

Jones contributions to the free energy were considered, as only these interactions are affected by the choice of bead type and the available experimental data for the side chain is for an uncharged residue. The results are presented in Figure S15. These results show that the SQ4p bead provides the closest match to experimental data with a calculated value of -22.95 kJ mol^{-1}, suggesting that this bead may be more appropriate to represent the guanidinium group in arginine. Therefore, this bead type was used for our CG model.

For the backbone beads (BB_1 and BB_2), the bead types suggested by the Martini 3 authors for a carboxylate group and primary amine group are Q5n and N6d, respectively. Therefore, the SQ5n bead type is used to represent the carboxylate group (a small bead size is used due to the 3-1 heavy atom to bead mapping) and the TN6d bead is used for the primary amine group (a tiny bead size is used due to the 2-1 heavy atom to bead mapping).

Pentaethylenehexamine is made up of 16 heavy atoms. Each end of the molecule terminates in a primary amine group, which is connected by repeating secondary amine

groups interspersed with two carbons. To maintain the symmetry of the molecule, each of these repeating units is represented by a single small Martini bead, while the end groups are represented by a tiny Martini bead representing the primary amine and nearest bonded carbon atom (as well as bonded hydrogen). The mapping scheme is presented in Figure S16.

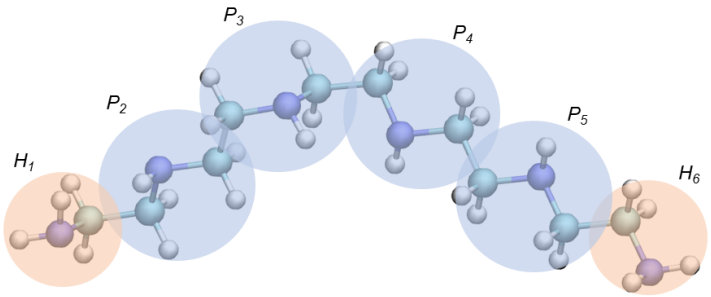

Figure S 16: Martini 3 mapping scheme for the PEHA molecule. Terminal primary amine groups with adjacent carbon are given the label H_1 and H_6 while secondary amine groups have labels P_{2-5}.

The bead type assignment for the chosen mapping is straightforward, since both primary and secondary amines have bead types recommended by the authors of the Martini 3 force-field [8]. The assignment is therefore only dependent on the charge state of the bead. For neutral primary amines and adjacent carbon (H_1 and H_6), with a 2-1 mapping, the TN6d bead type is recommended with the label representing the hydrogen bond donor characteristic of the amine group. When the terminal primary amine group is positively charged, the TQ5p bead is used instead. For the secondary amine groups and adjoining carbons (P_{2-5}), the SN4 bead type is recommended for neutral amine groups. While not explored in this work, the SQ2p bead could be used to represent positively charged secondary amine groups in PEHA, which occur at low pH [7]. The bead types assigned for both bio-inspired additives are summarised in Table S4.

Bonded parameters for the bio-inspired additives are determined from atomistic reference simulations as described in Section 2.4. Bonded parameters for bonds and angles are provided in Tables S5 and S6, respectively. For PEHA, calculated bond lengths and force constants for *H-P* and *P-P* bonds, and *H-P-P* and *P-P-P* angles, are averaged to a single value. Bonded parameters were generated using a single PEHA molecule with an overall neutral charge and the parameters are also used for CG models of charged PEHA molecules.

Table S 4: Summary of bead type assignments for PEHA and arginine.

Molecule	Bead	Charge	Bead Type
Arginine	BB_1	-1	SQ5n
	BB_1	0	SP2
	BB_2	0	TN6d
	BB_2	+1	TQ4p
	ARG_1	0	SC3
	ARG_2	+1	SQ4p
	ARG_2	0	SQ4p
PEHA	H	0	TN6d
	H	+1	TQ5p
	P	0	SN4
	P	+1	SQ2p

Table S 5: Bonded parameters for bio-inspired additive Martini 3 models. Bead names refer to labels in Figures S16 and S14. b_{ij} is the bond length and k_{ij} is the bond force constant.

Molecule	Bond	b_{ij} (nm)	k_{ij} (kJ mol^{-1})
Arginine	BB_1-BB_2	0.253	37000
	BB_2-ARG_1	0.363	4500
	ARG_1-ARG_2	0.387	9600
PEHA	H-P	0.308	6900
	P-P	0.368	9400

Table S 6: Angle type parameters for bio-inspired additive Martini 3 models. Bead names refer to labels in Figures S16 and S14. θ_{ijk} is the angle between beads and k_{ijk} is the angle force constant.

Molecule	Beads	θ_{ijk} (degrees)	Calculated k_{ijk} (kJ mol^{-1})
Arginine	BB_1-BB_2-ARG_1	84	60
	BB_2-ARG_1-ARG_2	141	44
PEHA	H-P-P	144	238
	P-P-P	146	384

.

S.5 Ionisation Model for Silicates

In order to account for the deprotonation of hydroxyl groups of silica oligomers at varying pH, a series of pKa values for each subsequent deprotonation needs to be determined. Each pKa value corresponds to the deprotonation of an exposed hydroxyl group bonded to a different silicon atom. The number of pKa values required is therefore equal to the number of silicon atoms in the oligomer (or in the case of the coarse-grained model, the number of silica beads). Note that this ignores the possibility of multiple hydroxyl groups bonded to a single silicon atoms becoming deprotonated which can occur in small oligomers. However, this only occurs at extremely high pH values [11], and therefore for simplicity this is not accounted for in this model.

Only very limited experimental data is available for the pKa values of silicate species. The most comprehensive review on the topic gives the required pKa values only for monomers and dimers [11]. However, the pKa value of a silica surface (that is, the surface of a significantly condensed silica network) is also known [12]. Therefore, a relationship can be devised between the number of silicate units in an oligomer and the pKa value of the first deprotonation. This function takes the form:

$$pKa = \frac{a}{b \times N_{Si} + 1} + 1.7i + 6.8 \tag{1}$$

where N_{Si} is the number of silicon units in the oligomer, i corresponds to the degree of deprotonation (i.e. $i = 1$ gives the pKa of the first deprotonation, $i = 2$ gives the pKa of the second deprotonation and so on) and a and b are parameters that are fitted to the known values for the first deprotonation of silica monomers and dimers. This function tends towards a minimum value of 6.8, the pKa of a silica surface, as the number of silicon units (N_{Si}) increases. The prefactor before the term i is the difference in pKa between the first and second deprotonation in dimers, and it is assumed that this difference is maintained for subsequent deprotonations in higher oligomers. The pKa values determined by this method for silica oligomers containing up to 8 silicon atoms (i.e. octamers) are given in Table S7 and Figure S17.

This model can be applied to approximate the proportion of silicate species of each degree of deprotonation for a given system pH. This is shown in Figure 18 for silica octamers between pH 7 and 15.

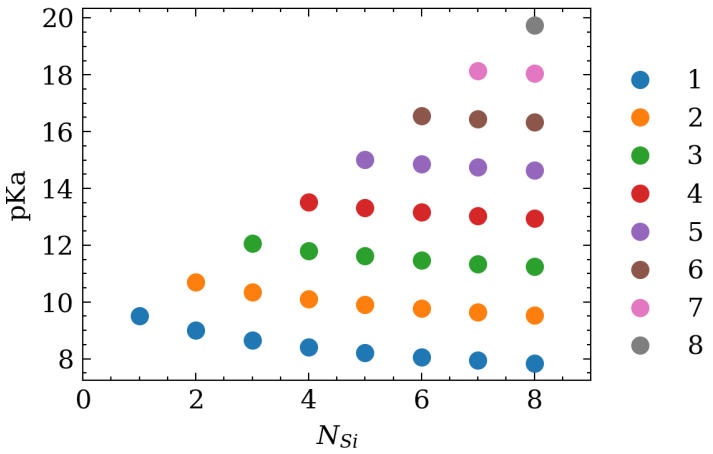

Figure S 17: Estimated pKa values for silica oligomers with up to 8 silicon units. The legend labels refer to the value of i, which is described by Eq.1.

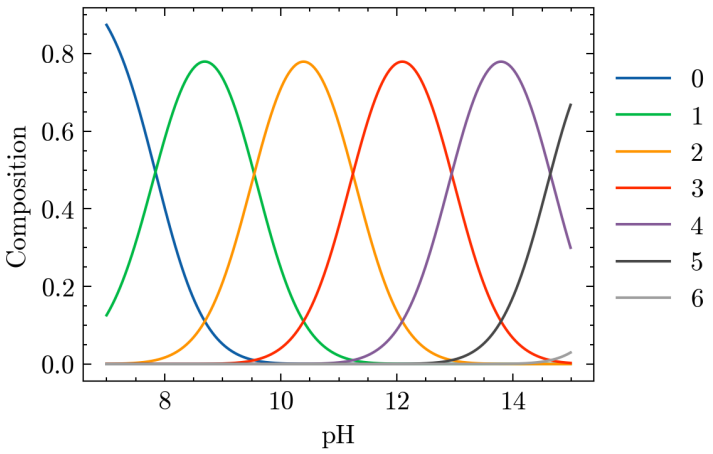

Figure S 18: Charge composition for silica octamers between pH 7 and 15. The legend labels refer to the total (negative) molecular charge.

Table S 7: Table of pKa values for silica oligomers with up to 8 silicon units. N_{Si} gives the number of silicon units while i corresponds to the degree of deprotonation. pKa values are calculated from Eq. 1.

		i							
		1	2	3	4	5	6	7	8
N_{Si}	1	9.50	-	-	-	-	-	-	-
	2	9.00	10.70	-	-	-	-	-	-
	3	8.68	10.38	12.08	-	-	-	-	-
	4	8.47	10.17	11.87	13.57	-	-	-	-
	5	8.30	10.00	11.70	13.40	15.10	-	-	-
	6	8.16	9.86	11.56	13.26	14.96	16.66	-	-
	7	8.05	9.75	11.45	13.15	14.85	16.55	18.25	-
	8	7.95	9.65	11.35	13.05	14.75	16.45	18.15	19.85

S.6 Simulation Details

Table S 8: Details of coarse-grained simulations carried out to investigate the effect of Si:CTAB ratio and pH on self-assembbly. N is the number of molecules of each species (denoted by the subscript) present in the simulation. Note that each water bead represents 4 water molecules. L is the box length in the x, y and z direction. t is the total simulation time.

Si:CTAB	pH	Box Type	N_{CTAB}	N_{SN1}	N_{SI1}	N_{SN8c}	$N_{SI8c(1-)}$	$N_{SI8c(2-)}$	$N_{SI8c(3-)}$	$N_{SI8c(4-)}$	N_{Br}	N_{TMA}	N_{Water}	L_x (nm)	L_y (nm)	L_z (nm)	t (µs)
0.5	13	Slab	1000	0	20	0	0	0	30	30	770	0	26000	22.4	22.4	7.5	3.0
1	13	Slab	1000	0	40	0	0	0	60	60	540	0	52000	31.6	31.6	6.9	3.0
2	13	Slab	1000	0	80	0	0	0	120	120	80	0	26000	22.4	22.4	7.5	3.0
4	13	Slab	1000	0	160	0	0	0	240	240	0	840	52000	31.6	31.6	7.1	3.0
8	13	Slab	1000	0	320	0	0	0	480	480	0	2680	104000	44.7	44.7	6.8	3.0
16	13	Slab	1000	0	640	0	0	0	960	960	0	6360	208000	63.3	63.3	6.7	3.0
2	10	Slab	1000	61	19	0	62	178	0	0	563	0	26000	22.4	22.4	6.8	3.0
4	10	Slab	1000	122	38	0	125	355	0	0	127	0	52000	31.6	31.6	7.1	3.0
8	10	Slab	1000	243	77	0	250	710	0	0	0	747	104000	44.7	44.7	6.8	3.0
16	10	Slab	1000	486	154	0	499	1421	0	0	0	2495	208000	63.3	63.3	6.7	3.0
2	7	Slab	1000	80	0	209	31	0	0	0	969	0	26000	22.4	22.4	6.8	3.0
4	7	Slab	1000	160	0	418	62	0	0	0	938	0	52000	31.6	31.6	7.1	3.0
8	7	Slab	1000	320	0	835	125	0	0	0	875	0	104000	44.7	44.7	6.8	3.0
16	7	Slab	1000	640	0	1670	250	0	0	0	750	0	208000	63.3	63.3	6.6	3.0

Table S 9: Details of coarse-grained simulations carried out with bio-inspired additives. N is the number of molecules of each species (denoted by the subscript) present in the simulation. Note that each water bead represents 4 water molecules. L is the box length in the x, y and z direction. t is the total simulation time.

Simulation	Box Type	N_{CTAB}	N_{SI2}	N_{Arg}	N_{PEHA}	N_{Water}	L_x (nm)	L_y (nm)	L_z (nm)	t (µs)
SI2	Elongated	1000	500	0	0	10000	8.2	8.2	27.3	6.0
Arg + SI2	Elongated	1000	500	250	0	10000	8.3	8.3	27.5	6.0
PEHA + SI2	Elongated	1000	500	0	250	13000	8.8	8.8	29.3	6.0

Table S 10: Details of atomistic simulations carried out with bio-inspired additives to determine coarse-grained model parameters. N is the number of molecules of each species (denoted by the subscript) present in the simulation. L is the box length in the x, y and z direction. t is the total simulation time.

Simulation	Box Type	N_{Arg}	N_{PEHA}	N_{Water}	L_x (nm)	L_y (nm)	L_z (nm)	t (ns)
Arginine	Elongated	1	0	874	3.0	3.0	3.0	50
PEHA	Elongated	0	1	2146	4.0	4.0	4.0	50

S.7 Additional Experimental Results

The organics content of the precipitate is strongly dependent on the Si:CTAB ratio, as shown in Figure S19. Synthesis carried out at a low Si:CTAB ratio, i.e. with a high concentration of surfactant species compared with the silica concentration, produced a precipitate with a high content of organic species, suggesting that additional surfactant molecules are bound to condensed silica when compared with syntheses where less surfactant is present. Sample 1-3 appears to be an outlier with a high organic content despite the high Si:CTAB ratio; however this can be explained by the extremely low quantity of material that was obtained under these synthesis conditions, which resulted in no measurable quantity of silica being present after calcination. Therefore, this sample is not shown in the plot of Figure S19.

A significantly higher organics content present in samples at a low Si:CTAB ratio (prior to calcination) indicates a greater surfactant uptake in the precipitated solid phase when the concentration of surfactant is increased. However, since this is not accompanied by an increase in yield of silica, this is more likely to be the result of surfactant rich assemblies that are bound to silica particles but do not possess sufficient silica to result in a porous solid being obtained after calcination. This is generally unfavourable, as the quantity of surfactant needed for these syntheses is much higher, without resulting in an increase in the quantity of mesoporous silica obtained. This is particularly pertinent when using calcination to remove the surfactant template from silica, as this bound surfactant is destroyed. Thus, a high ratio of Si:CTAB (and therefore a low concentration of CTAB) is desirable, particularly in terms of process scalability and economics.

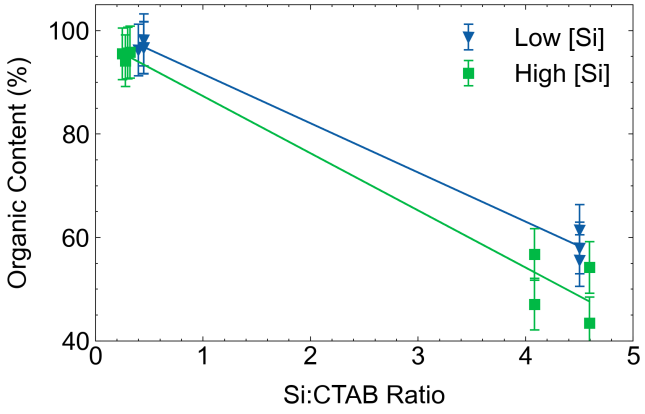

Figure S 19: Dependence of organic content on Si:CTAB ratio for all samples produced in the two-level four-factor factorial design. The line is a guide to the eye.

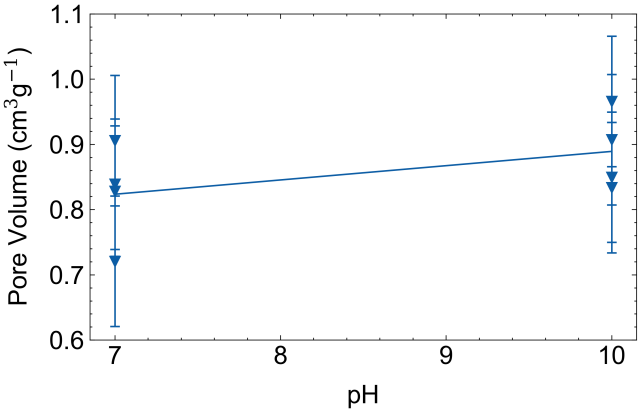

Figure S 20: Dependence of pore volume on pH. The line is a guide to the eye.

References

[1] J. S. Beck et al., 'A new family of mesoporous molecular sieves prepared with liquid crystal templates', *Journal of the American Chemical Society* **1992**, *114*, 10834–10843.

[2] C. T. Kresge, M. E. Leonowicz, W. J. Roth, J. C. Vartuli, J. S. Beck, 'Ordered mesoporous molecular sieves synthesized by a liquid—crystal template mechanism', *Nature* **1992**, *359*, 710–712.

[3] Q. Cai, W.-Y. Lin, F.-S. Xiao, W.-Q. Pang, X.-H. Chen, B.-S. Zou, 'The preparation of highly ordered MCM—41 with extremely low surfactant concentration', *Microporous and Mesoporous Materials* **1999**, *32*, 1–15.

[4] E. V. Vyshegorodtseva, Y. Larichev, G. V. Mamontov, 'The influence of CTAB/Si ratio on the textural properties of MCM—41 prepared from sodium silicate', *Journal of Sol-Gel Science and Technology* **2019**, *92*, 496–505.

[5] Y. Wang, L. Jiang, Q. Shen, J. Shen, Y. Han, H. Zhang, 'Investigation on the self—assembled behaviors of C 18 unsaturated fatty acids in arginine aqueous solution', *RSC Adv.* **2017**, *7*, 41561–41572.

[6] E. J. Shepherd, J. A. Kitchener, '474. The ionization of ethyleneimine and polyethyleneimine', *Journal of the Chemical Society (Resumed)* **1956**, 2448–2452.

[7] J. R. H. Manning, T. W. S. Yip, A. Centi, M. Jorge, S. V. Patwardhan, 'An Eco—Friendly, Tunable and Scalable Method for Producing Porous Functional Nanomaterials Designed Using Molecular Interactions', *ChemSusChem* **2017**, *10*, 1683–1691.

[8] P. C. T. Souza et al., 'Martini 3: a general purpose force field for coarse—grained molecular dynamics', *Nature Methods* **2021**, *18*, 382–388.

[9] R. Wolfenden, L. Andersson, P. M. Cullis, C. C. B. Southgate, 'Affinities of amino acid side chains for solvent water', *Biochemistry* **1981**, *20*, 849–855.

[10] A. Radzicka, R. Wolfenden, 'Comparing the polarities of the amino acids: side—chain distribution coefficients between the vapor phase, cyclohexane, 1—octanol, and neutral aqueous solution', *Biochemistry* **1988**, *27*, 1664–1670.

[11] J. Šefčík, A. V. McCormick, 'Thermochemistry of aqueous silicate solution precursors to ceramics', *AIChE Journal* **1997**, *43*, 2773–2784.

[12] S. Sjöberg, 'Silica in aqueous environments', *Journal of Non-Crystalline Solids* **1996**, *196*, 51–57.